Learning the Physics of Particle Transport via Transformers

Oscar Pastor-Serrano, Zoltán Perkó

Delft University of Technology,
Department of Radiation Science and Technology,
Mekelweg 15 2629JB Delft, Netherlands
o.pastorserrano@tudelft.nl

Abstract

Particle physics simulations are the cornerstone of nuclear engineering applications. Among them radiotherapy (RT) is crucial for society, with 50% of cancer patients receiving radiation treatments. For the most precise targeting of tumors, next generation RT treatments aim for real-time correction during radiation delivery, necessitating particle transport algorithms that yield precise dose distributions in sub-second times even in highly heterogeneous patient geometries. This is infeasible with currently available, purely physics based simulations. In this study, we present a data-driven dose calculation algorithm predicting the dose deposited by mono-energetic proton beams for arbitrary energies and patient geometries. Our approach frames particle transport as sequence modeling, where convolutional layers extract important spatial features into tokens and the transformer self-attention mechanism routes information between such tokens in the sequence and a beam energy token. We train our network and evaluate prediction accuracy using computationally expensive but accurate Monte Carlo (MC) simulations, considered the gold standard in particle physics. Our proposed model is 33 times faster than current clinical analytic pencil beam algorithms, improving upon their accuracy in the most heterogeneous and challenging geometries. With a relative error of $0.34 \pm 0.2\%$ and very high gamma pass rate of $99.59 \pm 0.7\%$ (1%, 3 mm), it also greatly outperforms the only published similar data-driven proton dose algorithm, even at a finer grid resolution. Offering MC precision 4000 times faster, our model could overcome a major obstacle that has so far prohibited real-time adaptive proton treatments and significantly increase cancer treatment efficacy. Its potential to model physics interactions of other particles could also boost heavy ion treatment planning procedures limited by the speed of traditional methods.

1 Introduction

Despite significant research efforts cancer remains a leading cause of death, responsible for more than 10 million deaths in 2020 worldwide (Ferlay et al. 2020; Sung et al. 2021). With more than 50% of the patients receiving radiation treatments, radiotherapy (RT) is at the forefront of current standard of care, playing a crucially important role in improving societal health. Sophisticated computational methods and particle transport simulations have been key to this success (Bernier, Hall, and Giaccia 2004), enabling highly personalized treatments. Traditional physics based algorithms improved all steps in the RT workflow (imaging, segmentation, dose calculation, optimization), but so far they proved too slow and inaccurate for real-time adaptive treatments promising ultimate precision with fewest adverse side-effects. Deep learning is key to overcome these limitations and realize the full potential of real-time adaptation.

Our study focuses on learning particle transport physics — fundamental to all steps of RT from Computed Tomography (CT) image reconstruction to simulating the actually delivered patient dose — to provide the necessary sub-second speed and high accuracy required for real-time adaptation. We frame the transport problem as sequence modelling, with a particle beam going through varying geometries and materials, using convolutional layers to learn relevant spatial features and the transformer self-attention mechanism to combine information from the feature tokens and a beam energy token. We train our algorithm to specifically learn proton transport in lung cancer patients with highly heterogeneous geometries to predict dose based on CT images alone, but the model could in theory be easily adapted to other particles (photons, electrons, heavy ions) and quantities (e.g., particle flux or secondary particle emission prediction).

Contributions Our specific contributions are as follows:

- We frame particle transport physics as a sequence modelling task and propose a novel algorithm using convolutional encoder and decoder layers together with transformer causal self-attention to predict dose distributions.
- We train our algorithm using highly variable geometries from lung cancer patients and demonstrate that it outperforms both current clinical pencil beam algorithms (PBA), being 33 times faster and more precise in the most complex geometries, and 'gold standard' Monte Carlo (MC) methods, offering MC accuracy 4000 times faster. Our model is also more accurate than the only published data driven proton dose calculation algorithm using (Long Short-Term Memory) LSTM cells.
- We highlight the direct societal impact of the presented algorithm by showcasing how it could improve current radiotherapy practice and enable real-time adaptive treatments. While we train our model to learn proton physics

to predict dose distributions, we also detail extensions to make it a general particle transport simulator, accounting for e.g., beam shape or energy spectrum changes.

2 Background

Here we describe RT workflow and the critical role of particle transport and dose calculation methods, and frame our work in terms of unsolved challenges and related literature.

Radiotherapy workflow RT treatments usually follow a 4-step procedure. First, high quality anatomical information is acquired — typically as CT images (Pereira, Traughber, and Muzic 2014) — on which target tumors and organs at risk (OARs) to protect are delineated. Second, the irradiation modality is chosen, with most patients receiving photon treatments, but proton therapy spreading quickly due to protons' finite range and significantly better ability to focus dose on tumors (Lundkvist et al. 2005). Third, a treatment plan is obtained, containing the intensities, energies and angles of the thousands of pencil beams used for irradiation. This is the most complex and computationally expensive task, requiring solving large scale multi-criteria optimization problems and calculating the dose deposited by each individual pencil beam before an acceptable, clinically 'best' plan is achieved (Hussein et al. 2018; Meyer et al. 2018). Last, for quality assurance purposes detailed dose calculations are performed to test plan robustness against anatomical changes or decide to adapt a plan for future irradiations.

Particle transport & dose calculation Accurate particle transport algorithms are crucial for all these steps. CT image reconstruction relies on simulating photon interactions with tissues and detectors; plan optimization requires the spatial dose distribution (typically in more than 1 million voxels) from each available proton or photon beamlet (in the thousands); while for plan evaluation the dose must be calculated for many different geometries. Ideally these calculations should be quick and precise, but current analytical pencil beam algorithms and stochastic MC dose calculation tools offer a trade-off. PBA yields results without the computational burden of MC engines, but its accuracy is severely compromised in highly heterogeneous or complex geometries, making slow and clinically rarely affordable MC approaches necessary. The problem is most acute for next generation real-time adaptive treatments promising ultimate precision with fewest side effects by correcting treatments during irradiation, e.g., to account for anatomical changes due to breathing, coughs or intestinal movements. To finally become reality, such adaptive treatments require algorithms that deliver MC accuracy in sub-second speed.

Related work Deep learning has achieved significant improvements in all steps of the RT workflow (Meyer et al. 2018), but only imaging, treatment planning and dose calculation are relevant to our work. U-net (Ronneberger, Fischer, and Brox 2015) and Generative Adversarial Networks (Goodfellow et al. 2014) (and their variants) have been widely applied to improve image quality, e.g., to generate synthetic CT images from Magnetic Resonance Images (offering better soft tissue contrast than CT without additional patient dose) or low dose Cone-Beam CT (CBCT) images (Edmund and Nyholm 2017; Zhang et al. 2021); to predict stopping power from CBCT (Harms et al. 2020); or correct scatter artifacts in CBCT reconstruction (Lalonde et al. 2020). These works represent image to image transformation, producing more useful images for the RT workflow than their easier/faster to obtain or lower patient dose input.

In treatment planning, deep learning methods aim to predict an optimal 3D patient dose distribution based on historical data. The most successful works use ResNet (Chen et al. 2019; Fan et al. 2019), 2/3D U-net (Kearney et al. 2018; Nguyen et al. 2019b; Kajikawa et al. 2019) or hierarchically densely connected U-net (HDU-net) (Nguyen et al. 2019a; Barragán-Montero et al. 2019) architectures, with segmented structure masks as input. Some also utilize the CT image (Kearney et al. 2018) and manually encoded beam configuration information (Nguyen et al. 2019a; Barragán-Montero et al. 2019). These works basically mimic 'optimal' plans for new patients that should be achievable based on past ones, only outputting final dose distributions, but not the required beam intensities (i.e., fluence maps) needed to deliver such plans, which must be obtained via additional, costly optimization. Thus, they are mostly used for Quality Assurance (QA) purposes to aid planning, not replace it. Only few papers attempt to jointly predict dose distribution and fluence maps (Lee et al. 2019; Wang et al. 2020), and all have been applied to photon treatments.

Practically all applications of deep learning to dose calculations learn how to improve cheaper and faster physics based simulations. Most works try to predict low noise MC photon dose distributions from high noise MC doses (Peng et al. 2019a,b; Bai et al. 2021; Neph et al. 2021), or deterministic particle transport based photon distributions from simple analytical calculations (Xing et al. 2020b; Dong and Xing 2020), using CNNs, U-net or HDU-net architectures with 2/3D patches. A few papers manually encode some physics information as additional input such as fluence maps (Fan et al. 2020; Xing et al. 2020a), total energy released per unit mass maps (Zhu, Liu, and Chen 2020) or beam information (Kontaxis et al. 2020; Tsekas et al. 2021). We are only aware of 2 papers (Wu et al. 2021; Javaid et al. 2021) using deep learning to predict accurate low noise MC proton dose distributions, both using cheap physics models (noisy MC and PBA) as input. While all these works provide significant speed-up compared to pure physics based algorithms, some even reaching sub-second speeds, they all require physics models to produce their input, do not generalize easily (e.g., to different beam energies) and are trained with full plan data, unsuitable for real-time adaptation needing the individual dose distribution from each beamlet alone.

Most related to ours is the work from (Neishabouri et al. 2021), using LSTM networks to sequentially calculate proton pencil beam dose distributions from relative stopping power slices. Although requiring a separate model per beam energy, this LSTM-based dose engine offers excellent inference times and close to PBA accuracy when tested on external patient data. Our approach builds upon the methodology of (Neishabouri et al. 2021), but uses a different architecture, works on finer resolution and — most crucially — also learns the physics of energy dependence in particle transport via a single model.

Transformer The backbone of the presented model is the Transformer, introduced by (Vaswani et al. 2017) for machine translation tasks. The Transformer and similar attention-based frameworks have completely replaced recurrent architectures like LSTM in natural language processing applications since then (Devlin et al. 2019; Brown et al. 2020). One reason behind their large-scale adoption and success is the ability to process long-term dependencies by directly accessing information at any point in the past without needing internal memory, which is essential to introduce beam energy dependence in our model.

Transformer-based architectures have also achieved state-of-the-art performance in computer vision tasks like image classification (Ramachandran et al. 2019; Dosovitskiy et al. 2020). Inspired by (Cordonnier, Loukas, and Jaggi 2019), (Dosovitskiy et al. 2020) present the Vision Transformer (ViT), circumventing the quadratic cost of computing the attention weight matrix by dividing the input image into a patch sequence. Following the Transformer basis of ViT, our model also adopts a patch-based processing of the inputs.

The price Transformers pay for their generality in both language and computer vision is the need for a self-supervised pre-training stage with large amounts of text or image data (Devlin et al. 2019; Brown et al. 2020; Dosovitskiy et al. 2020). For image classification, several approaches try to achieve state-of-the-art performance without costly pre-training (Touvron et al. 2020; D'Ascoli et al. 2021). As in the concurrent work of (Hassani et al. 2021), our model can be directly trained on a relatively small dataset by using a convolutional encoder first extracting important features from the patched input data.

Self-attention The proposed model leverages the self-attention (SA) mechanism (Vaswani et al. 2017) allowing dynamic routing of information between the L elements in a sequence $\boldsymbol{z} \in \mathbb{R}^{L \times D}$. SA is based on the interaction between a series of queries $\boldsymbol{Q} \in \mathbb{R}^{L \times D_h}$, keys $\boldsymbol{K} \in \mathbb{R}^{L \times D_h}$, and values $\boldsymbol{V} \in \mathbb{R}^{L \times D_h}$ obtained through a learned linear transformation of the input sequence

$$[\boldsymbol{Q}, \boldsymbol{K}, \boldsymbol{V}] = \boldsymbol{z}\boldsymbol{W}_{QKV}, \tag{1}$$

with learned weights $\boldsymbol{W}_{QKV} \in \mathbb{R}^{D \times 3D_h}$. Intuitively, every sequence element emits a query and a key vector with the information to gather from and to offer to the rest of the sequence, respectively. Each of the L elements in the output sequence is a weighted sum of the values, where the weights — referred to as attention matrix $\boldsymbol{A} \in \mathbb{R}^{L \times L}$ — are obtained by matching queries against key vectors via inner products

$$\boldsymbol{A} = \text{softmax}\Big(\frac{\boldsymbol{Q}\boldsymbol{K}^T}{\sqrt{D_h}}\Big), \tag{2}$$

$$\text{SA}(\boldsymbol{z}) = \boldsymbol{A}\boldsymbol{V}. \tag{3}$$

Multi-head self-attention (MSA) runs N_h parallel SA operations to extract different features and inter-dependencies, translating into setting $D = D_h \cdot N_h$. The outputs of the different operations, called *heads*, are concatenated and are linearly projected with learned weights $\boldsymbol{W}_h \in \mathbb{R}^{N_h D_h \times D}$ as

$$\text{MSA}(\boldsymbol{z}) = \underset{h \in \{N_h\}}{\text{concat}} [\text{SA}_h(\boldsymbol{z})] \boldsymbol{W}_h. \tag{4}$$

By definition, MSA is invariant to the relative order of elements in the sequence. To account for positional information, fixed (Vaswani et al. 2017) or learned (Dosovitskiy et al. 2020) positional embedding can be added or concatenated to the input right before the first MSA operation. In addition, in MSA every element in the sequence can retrieve information at any past and future point. For some prediction tasks where the elements cannot or need not attend to future information, a binary mask is used to stop information flow from the future to the present. Such SA mechanism variant is referred to as causal SA and is particularly suited for modeling proton interactions and energy deposition physics that mostly occur sequentially in the forward beam direction.

3 Methods

Our objective is sub-second prediction of the dose deposited by individual proton beamlets via a model that implicitly captures the physics of particle transport. The presented transformer-based parametric model exploiting the forward sequential nature of proton transport physics is well-suited for this. This section describes the model's building blocks, the dataset and the training and evaluation procedures.

Proposed model We introduce a parametric model that computes the output dose distribution $\boldsymbol{y} \in \mathbb{R}^{L \times H \times W}$ given the input geometry data $\boldsymbol{x} \in \mathbb{R}^{L \times H \times W}$ and particle energy $\epsilon \in E \subset \mathbb{R}^+$, where L is the depth, H is the height and W is the width of the geometric 3D grid. The model — referred to as Dose Transformer Algorithm (DoTA) — captures the relationship between the inputs and the output dose distribution through a nonlinear mapping $f_{\boldsymbol{\theta}}(\boldsymbol{x}, \epsilon)$: $\mathbb{R}^{L \times H \times W} \times E \rightarrow \mathbb{R}^{L \times H \times W}$, performed by a series of artificial neural networks. Figure 1 shows the architecture of the model, which processes the 3D input geometry $\boldsymbol{x}$ as a sequence of L 2D images in the beam's eye view $\{\boldsymbol{x}_i | \boldsymbol{x}_i \in \mathbb{R}^{1 \times H \times W}, \forall i = 1, ..., L\}$.

Convolutional encoder First, a convolutional encoder extracts important features such as geometry contrasts and edges from the input CT slices. The convolutional encoder contains two blocks, each with a convolutional, a Group Normalization (GN) (Wu and He 2020) and a pooling layer, followed by a Rectified Linear Unit (ReLU) activation. After the second block, a convolution with K filters results in a sequence of elements of reduced embedding dimension $D = H' \times W' \times K$, where H' and W' are the reduced height and width of the images. The layers in the convolutional encoder share weights and are applied independently to every element $\boldsymbol{x}_i$ in the sequence. We refer to the output of the convolutional encoder as tokens $\{\boldsymbol{z}_i | \boldsymbol{z}_i \in \mathbb{R}^D, \forall i = 1, ..., L\}$.

Transformer encoder The interaction between tokens $\boldsymbol{z}_i$ is modeled in the transformer encoder through causal MSA, with each token routing information from all preceding tokens. To account for the relative positional information of

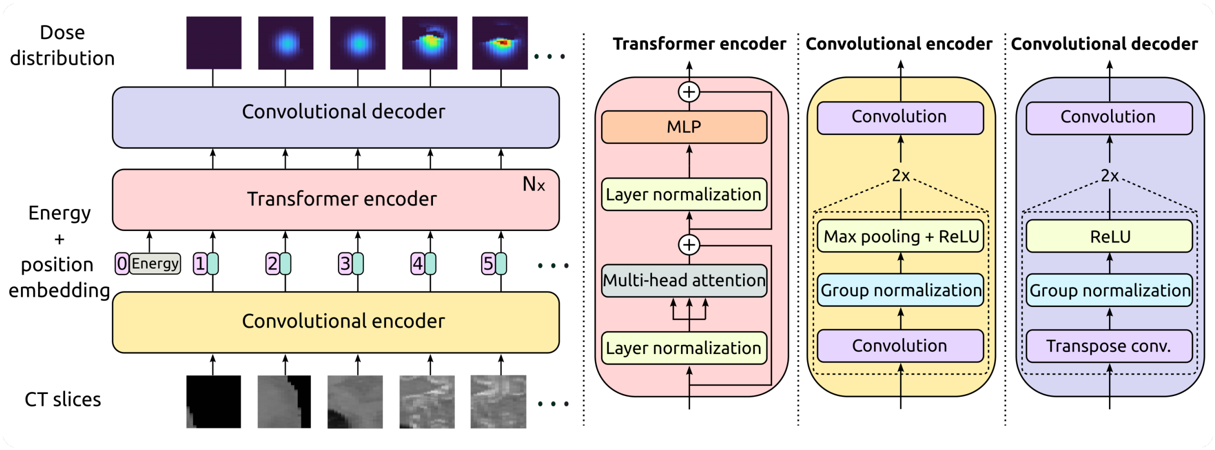

Figure 1: Model architecture. We treat the input and output 3D volumes as a sequence of 2D slices. A convolutional encoder reduces the dimension of the input and extracts important geometrical features. The particle energy is added at the beginning of the resulting sequence. A transformer encoder with causal self-attention then routes information between the encoded input slices. Finally, a convolutional decoder transforms the low-dimensional sequence into an output sequence of 2D dose slices.

sequence elements we add a learnable embedding to each token. We include an extra energy token $\boldsymbol{z}_e = \boldsymbol{W}_e \epsilon \in \mathbb{R}^D$ at the beginning of the sequence, where $\boldsymbol{W}_e \in \mathbb{R}^{D\times 1}$ is a learned linear projection of the beam energy ϵ. The transformer encoder alternates MSA and Multi-layer Perceptron (MLP) layers, with Layer Normalization (LN) applied before every layer (Ba, Kiros, and Hinton 2016) and residual connections after every layer. A stack of N transformer encoder blocks computes the operations

$$\boldsymbol{z}_0 = [\boldsymbol{z}_e; \boldsymbol{z}] + \boldsymbol{r}_p, \tag{5}$$

$$\boldsymbol{s}_n = \boldsymbol{z}_{n-1} + \text{MSA}(\text{LN}(\boldsymbol{z}_{n-1})), \qquad n = 1 \ldots N \tag{6}$$

$$\boldsymbol{z}_n = \boldsymbol{s}_n + \text{MLP}(\text{LN}(\boldsymbol{s}_n)), \qquad n = 1 \ldots N \tag{7}$$

where $\boldsymbol{r}_p \in \mathbb{R}^{(L+1)\times D}$ is the learnable positional embedding and MLP is a two layer feed-forward network with Dropout (Srivastava et al. 2014) and Gaussian Error Linear Unit (GELU) activations (Hendrycks and Gimpel 2016).

Convolutional decoder To produce output dose volume $\boldsymbol{y}$ with the same dimension as the input, each token is transformed via a convolutional decoder with shared weights into the output slices $\{\boldsymbol{y}_i | \boldsymbol{y}_i \in \mathbb{R}^{1\times H\times W}, \forall i = 1, ..., L\}$. Instead of normal convolutional layers, the decoder contains transposed convolutions that increase the dimension of their input. Similarly to the convolutional encoder, two final dimension-preserving convolutions transform the output of the second block into the 2D dose slices.

Dataset The models are trained using a dataset with pairs of sliced CT images and dose distributions corresponding to mono-energetic proton beams with different energies. The 3D CT scans from 4 lung cancer patients are highly heterogeneous due to the air, bones and organs present in the thorax, and cover a volume of $512 \times 512 \times 100$ mm^3 with a resolution of $1 \times 1 \times 3$ mm. Since each proton beam has approximately 20 mm diameter and travels up to 250 mm through a small volume only, we crop and extract blocks $\boldsymbol{x} \in \mathbb{R}^{256\times 48\times 16}$ maintaining the original CT resolution. Many different blocks can be obtained from the same patient by rotating the CT scan along the Z direction in steps of 5° and applying shifts in YZ plane with 5 mm steps.

The output ground-truth dose distributions are calculated using the open source Monte Carlo particle transport software MCsquare (Souris, Lee, and Sterpin 2016), taking CT slices and calculating output blocks $\boldsymbol{y} \in \mathbb{R}^{256\times 48\times 16}$ with the same size and resolution as the input via random sampling of proton trajectories. Dose distributions are estimated using 3 million primary particles ensuring low MC noise levels of 0.6%. For each input CT block we generate 4 dose distributions corresponding to 4 randomly sampled energies between 80 and 130 MeV, rounded to 1 decimal. We mask MC noise by zeroing out dose values below the noise level.

The entire training dataset consists of 63,048 pairs of input-output blocks, 10% of which are used as a validation set. We apply data augmentation during training and randomly rotate the volumes 180° in beam's eye view (YZ plane), doubling the number of samples. A test set of 3,618 input-output pairs from an additional 5th patient is used to evaluate generalization to unseen geometries and energies.

Training details The best performing model consists of one transformer encoder block with 16 heads and convolutional layers with a 3×3 kernel. Using size preserving zero-padding results in halving (or doubling, for the decoder) the H and W dimensions after each convolutional block. The token embedding dimension $D = H/4 \times W/4 \times K$ is constant throughout the transformer encoder layers, with height $H = 48$, width $W = 16$, $K = 10$ kernels and $D = 480$ in our particular case. The models are trained with Tensorflow (Abadi et al. 2015) using the LAMB optimizer (You et al. 2019) and mini-batches of 8 samples, limited by the maximum internal memory of the Nvidia Tesla T4® Graphics Processing Unit (GPU) used during our experiments. We use the mean squared error (MSE) as loss function and a scheduled learning rate starting at 10^{-3} that is halved every 4 epochs. In Appendix A we perform a model hyperparameter search varying the number of transformer layers N, convolutional filters K and attention heads N_h.

Gamma analysis We compare the predicted and ground-truth 3D dose distributions from the test set using gamma analysis (Low et al. 1998). Intuitively, for a set reference points and their corresponding reference dose values, this method searches for similar dose values within small spheres around each point. The similarity is quantified using a maximum dose difference threshold (usually expressed as a percentage of the reference dose): e.g., dose values are accepted similar if within 1% of the reference dose. The radius of the sphere is referred to as distance-to-agreement criterion. Mathematically, gamma values are calculated for individual points in the predicted dose grid as

$$\gamma(\boldsymbol{p}) = \min_{\hat{\boldsymbol{p}}}\{\Gamma(\boldsymbol{p}, \hat{\boldsymbol{p}})\}, \tag{8}$$

$$\Gamma_{\delta,\Delta}(\boldsymbol{p}, \hat{\boldsymbol{p}}) = \sqrt{\frac{|\boldsymbol{p} - \hat{\boldsymbol{p}}|^2}{\delta^2} + \frac{|D(\boldsymbol{p}) - D(\hat{\boldsymbol{p}})|^2}{\Delta^2}}, \tag{9}$$

where $\boldsymbol{p}$ are the coordinates of the points in the predicted dose grid and $\hat{\boldsymbol{p}}$ the coordinates of the points in the ground truth dose grids. $D(\boldsymbol{p})$ is the dose at any point $\boldsymbol{p}$, δ is the distance-to-agreement and Δ the dose difference criterion.

We use the publicly available gamma evaluation functions from PyMedPhys[1], with $\delta = 3$ mm and $\Delta = 1\%$. The 3 mm distance-to-agreement criterion ensures a neighborhood search of at least one voxel, while the dose difference criterion of 1% disregards uncertainty due to MC noise. Gamma values are calculated for each voxel and a voxel centered at $\boldsymbol{p}$ is considered to pass the gamma evaluation if $\gamma(\boldsymbol{p}) < 1$. For the entire grid, the gamma pass rate can be calculated as the fraction of passed voxels over total number of voxels.

Error analysis The sample average relative error is used as an additional method to explicitly compare dose differences between two grids. Given the predicted output $\boldsymbol{y}$ and the ground truth dose distribution $\hat{\boldsymbol{y}}$, the average relative error ρ can be calculated as

$$\rho = \frac{\|\boldsymbol{y} - \hat{\boldsymbol{y}}\|_{L_1}}{\max_j \hat{\boldsymbol{y}}_j} \times 100, \tag{10}$$

where $\max_j \hat{\boldsymbol{y}}_j$ is the maximum dose value among all voxels in the ground-truth dose grid.

4 Experiments

We compare the performance of the presented DoTA model to both state-of-the-art and clinically used methods. The experiments first focus on evaluating the accuracy all models: the gamma evaluation serves as a tool to assess dosimetric differences, while the relative error allows direct comparison of the predicted output and ground truth grids. Last, we report calculation times and evaluate DoTAs' potential to displace other algorithms as a fast dose calculation tool.

Baselines Our approach is compared to PBAs, the group of analytical dose calculation methods mostly used in the clinic. In particular, we calculate dose distributions for the entire test set using the PBA included in the open-source treatment planning software matRad[2] (Wieser et al. 2017). The DoTA model is also compared to the only published data-driven approach based on LSTM cells (Neishabouri et al. 2021). Since the LSTM models in (Neishabouri et al. 2021) are trained for a single energy, we additionally train a model using 104.25 megaelectronvolt (MeV) proton beams.

Gamma evaluation The gamma pass rate is calculated for every test sample using the MC dose distributions as reference with two settings. In the first *unmasked* setting identical to (Neishabouri et al. 2021), voxels with exactly 0 gamma value are excluded from the pass rate calculation. These are typically voxels not receiving any dose in both the predicted and ground-truth grids, having no clinical relevance. However, the outputs of the model's last linear layer are hardly ever exactly 0, taking very small values instead. Thus, in the second, stricter *masked* setting, we mask voxels in the predicted dose grid that are below 0.01% of the maximum dose.

Table 1 summarizes the results of the gamma evaluation for both settings. We report mean, standard deviation, maximum and minimum pass rates across the entire test set. Even with energy dependence and a finer grid resolution, DoTA outperforms the LSTM model in all aspects: the average pass rate is higher, the spread lower, and the minimum is almost 2% higher. The performance of PBA and DoTA is very similar: their average values are very close in both the masked and unmasked setting, and their gamma pass rate distributions (left plot of Figure 2) almost overlap. The minimum pass rate is significantly higher for DoTA, indicating that PBA struggles with the most heterogeneous and complicated samples. To verify this, we divide the dose beamlet into 4 equal sections along depth and score the number of failed voxels per section across the entire test set. The right plot in Figure 2 shows the proportion of voxels failing the gamma evaluation per section, out of the total number of failed voxels. The higher proportion in the 4th, last section of the beam represents inaccuracies in the high dose, clinically most relevant regions where the effects of heterogeneities are most evident.

Error evaluation To explicitly compare the performance of PBA and DoTA, we calculate the sample average relative error ρ of the test set. Table 2 shows the mean, standard deviation, maximum and minimum errors observed across all test samples, and the left plot in Figure 3 displays the distribution of ρ values for both models. Though PBA achieves low errors in the most homogeneous samples, our approach is clearly superior with a lower mean ρ and a twice lower maximum error. The depth profile in the right plot of Figure 3 shows the same trend as the gamma evaluation: DoTA outperforms PBA in the last high dose regions of the beam.

Time evaluation Besides high prediction accuracy, fast inference times are critical for clinical dose calculation algorithms. Table 3 reports run times of the LSTM, DoTA, PBA

[1] see https://docs.pymedphys.com

[2] Available at https://github.com/e0404/matRad.

Table 1: Gamma analysis results ($\delta = 3\text{mm}$, $\Delta = 1\%$). For PBA and DoTA, gamma pass rates are calculated across the same test set. Pass rates of the LSTM models are directly obtained from (Neishabouri et al. 2021). Mask indicates whether the predicted low dose values below 0.01% of the maximum dose are masked before gamma evaluation. Mean, standard deviation (Std), minimum (Min) and maximum (Max) values across the test set are shown for each model, mask and energy combination.

Model	Mask	Energy (MeV)	Mean (%)	Std (%)	Min (%)	Max (%)
LSTM (Neishabouri et al. 2021)	✗	67.85	98.56	1.30	95.35	99.79
	✗	104.25	97.74	1.48	92.57	99.74
	✗	134.68	94.51	2.99	85.37	99.02
DoTA (ours)	✗	104.25	99.55	0.71	93.45	100
	✗	[80, 130]	99.59	0.70	92.79	100
	✓	[80, 130]	99.12	1.45	87.32	100
PBA (Wieser et al. 2017)	✗	[80, 130]	99.45	1.16	89.61	100
	✓	[80, 130]	99.16	1.73	83.35	100

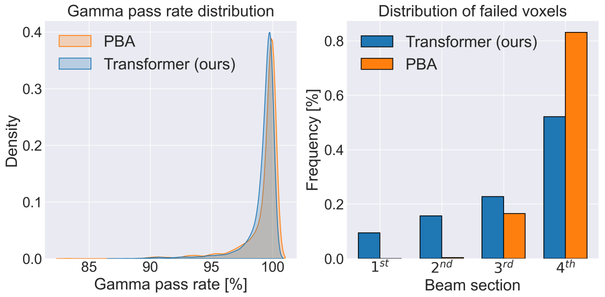

Figure 2: (Left) Distribution of the gamma pass rates across the test set for the PBA and DoTA. (Right) Distribution of the failed voxels along the beam, where each bin shows the ratio between the number of voxels in the test set that fail the gamma evaluation within a section of the beam and the total number of failed voxels.

Table 2: Average relative error between predicted and reference MC dose distributions. Reported values include mean, standard deviation (Std), minimum (Min) and maximum (Max) values across the test set, for both the PBA and DoTA.

Model	Mean (%)	Std (%)	Min (%)	Max (%)
DoTA (ours)	0.3430	0.1999	0.0780	1.4250
PBA	0.3863	0.3154	0.0683	2.7317

and MC dose algorithms. Though dependent on hardware, the data-driven approaches are clearly faster than clinically used PBA and MC baselines. While LSTM seems faster than DoTA, this is partially due to the LSTM model having 2.67 times smaller input/output and being run on better hardware. Our proposed approach offers a 33 compared to PBAs and 4000 times speed-up with respect to MC methods.

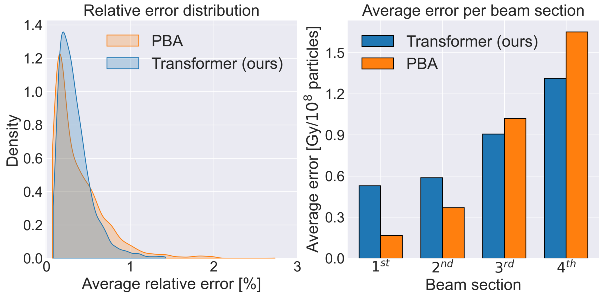

Figure 3: (Left) Distribution of the average relative errors across the test set for the PBA and DoTA. (Right) Comparison of the average relative error per beam section, where each bin shows the mean relative error across the test set for equally sized sections of the beam.

Table 3: Mean inference time and standard deviation (Std) across the test set for each model. Reported run times only account for the dose calculation and disregard preprocessing steps. The values for the LSTM model are taken directly from (Neishabouri et al. 2021). The DoTA runtimes include the per-sample runtime obtained using the maximum GPU capacity corresponding to a batches of 8 sample.

Model	Mean (ms)	Std (ms)
LSTM[a]	6.0	-
DoTA[b] (1 per batch)	70.5	10.2
DoTA[b] (8 per batch)	31.2	1.0
PBA[c]	1,030.7	108.9
MC[c]	128,948.5	31,708.8

[a] Nvidia® Quadro RTX 6000 64 Gb RAM
[b] Debian10 4 vCPUs 15 Gb RAM - Nvidia® Tesla T4 16 Gb RAM
[c] Ubuntu 20.04 intel® Core™ i7-8550U 1.8 GHz 16Gb RAM

Additional geometries Figure 4 displays the worst performing test sample in terms of gamma pass rate for the PBA and DoTA models. Both samples consist of a beam traversing the lungs, where most of the energy is deposited in a highly heterogeneous region, with the PBA sample completely misplacing the high energy peak, while DoTA still yielding reasonable prediction. In Appendix B we evaluate the model in additional geometries unseen during training.

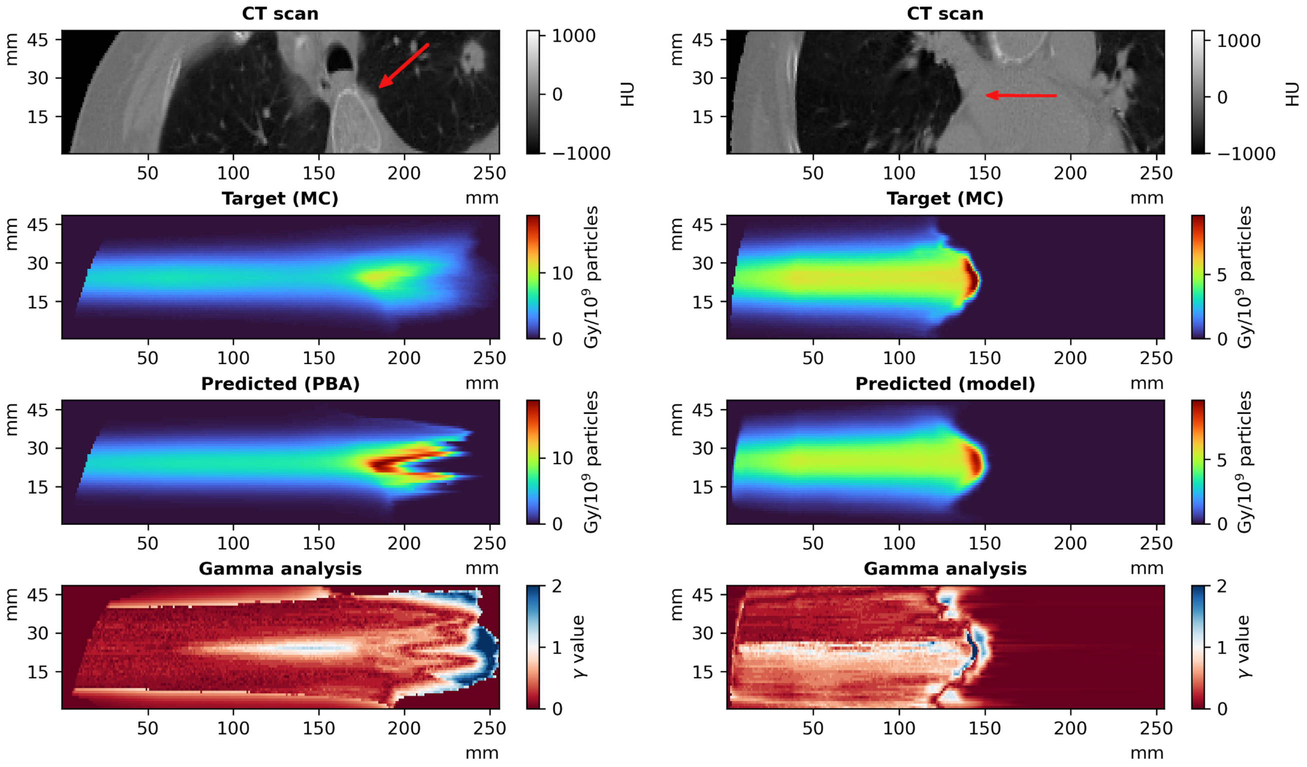

(a) PBA

(b) DoTA

Figure 4: Worst performing sample in the gamma evaluation across the test set, for (a) PBA and (b) DoTA. Each plot displays the central slice of the 3D input CT grid, the MC ground truth dose distribution, the model prediction and the gamma values.

5 Conclusions

After their recent success in natural language processing and computer vision tasks, transformer-based architectures prove to excel in problems that involve sequential image processing too. Framing particle transport as sequence modeling of 2D geometry slices, we use their power to build a fast and accurate dose calculation algorithm that implicitly learns proton transport physics and has the potential for profound social impact by enabling next generation, real-time adaptive radiotherapy cancer treatments.

Our evaluation shows that the presented DoTA model has the right attributes to replace proton dose calculation algorithms currently used in clinical practice. Compared to PBAs, DoTA achieves 33x faster inference times while being better suited for heterogeneous patient geometries. The high gamma pass rate in unseen geometries from an external patient also demonstrate that the model predicts close to high accuracy MC dose distributions in sub-second times.

Such speed and accuracy increase could directly improve current RT practice by allowing comprehensive plan robustness analysis (now performed by checking only few potential geometries), quick dosimetric quality assurance of daily treatments (mostly done by analysing anatomy changes via comparing pre-treatment CT/CBCT images to the planning CT instead of corresponding dose distributions variations) and precise evaluation of needing plan adaptation. Crucially, the sub-second speed for individual pencil beam dose calculation and incorporation of energy dependence make our model well suited for real-time treatment adaptation.

To our knowledge DoTA is the first deep learning method to implicitly learn particle transport physics, predicting dose using only CT and beam energy as input, as opposed to previous works only learning corrections for 'cheap' physics based predictions or predicting dose under fixed conditions. The flexibility to incorporate additional beam characteristics, e.g., changes in beam shape (provided as 0th image slice) or energy spectrum (as the ϵ 0th token), or to predict additional quantities (e.g., particle flux) holds the potential to be a fast, general particle transport algorithm. Since photons (used in photon therapy and CT/CBCT imaging) and heavy ions (in carbon and helium therapy) share similar, mostly forward scatter physics, training our algorithm for different particles could open door to several further applications: e.g., predicting physical or radiobiological dose (requiring DNA scale simulations) in heavy ion treatments (yielding higher speed-ups due to the longer computations); or real-time CBCT image reconstruction to provide input for real-time adaptation. Attending to future information too could even allow learning large angle scatter physics crucial for electron therapy. Thus, the presented algorithm could significantly contribute to improving cancer treatments, having profound societal impact even on the short term.

Acknowledgments

The authors would like to thank Kevin Wielinga for his contributions to this project. This work is supported by KWF Kanker Bestrijding [grant number 11711], and is part of the KWF research project PAREL. Zoltán Perkó would like to thank the support of the NWO VENI grant ALLEGRO (016.Veni.198.055) during the time of this study.

Code availability

The code, weights and results are publicly available at https://github.com/ (to be released with camera-ready version).

CRediT authorship contribution statement

Oscar Pastor-Serrano: Conceptualization, Methodology, Software, Validation, Formal Analysis, Investigation, Data Curation, Writing – original draft, Visualization.
Zoltán Perkó: Conceptualization, Methodology, Formal Analysis, Resources, Writing – original draft, Writing – Review & editing, Supervision, Project Administration, Funding Acquisition.

References

Abadi, M.; Agarwal, A.; Barham, P.; Brevdo, E.; Chen, Z.; Citro, C.; Corrado, G. S.; Davis, A.; Dean, J.; Devin, M.; Ghemawat, S.; Goodfellow, I.; Harp, A.; Irving, G.; Isard, M.; Jia, Y.; Jozefowicz, R.; Kaiser, L.; Kudlur, M.; Levenberg, J.; Mané, D.; Monga, R.; Moore, S.; Murray, D.; Olah, C.; Schuster, M.; Shlens, J.; Steiner, B.; Sutskever, I.; Talwar, K.; Tucker, P.; Vanhoucke, V.; Vasudevan, V.; Viégas, F.; Vinyals, O.; Warden, P.; Wattenberg, M.; Wicke, M.; Yu, Y.; and Zheng, X. 2015. TensorFlow: Large-Scale Machine Learning on Heterogeneous Systems. Software available from tensorflow.org.

Ba, J. L.; Kiros, J. R.; and Hinton, G. E. 2016. Layer Normalization.

Bai, T.; Wang, B.; Nguyen, D.; and Jiang, S. 2021. Deep dose plugin: towards real-time Monte Carlo dose calculation through a deep learning-based denoising algorithm. *Machine Learning: Science and Technology*, 2(2): 025033.

Barragán-Montero, A. M.; Nguyen, D.; Lu, W.; Lin, M.-H.; Norouzi-Kandalan, R.; Geets, X.; Sterpin, E.; and Jiang, S. 2019. Three-dimensional dose prediction for lung IMRT patients with deep neural networks: robust learning from heterogeneous beam configurations. *Medical Physics*, 46(8): 3679–3691.

Bernier, J.; Hall, E. J.; and Giaccia, A. 2004. Radiation oncology: a century of achievements. *Nature Reviews Cancer*, 4(9): 737–747.

Brown, T. B.; Mann, B.; Ryder, N.; Subbiah, M.; Kaplan, J.; Dhariwal, P.; Neelakantan, A.; Shyam, P.; Sastry, G.; Askell, A.; Agarwal, S.; Herbert-Voss, A.; Krueger, G.; Henighan, T.; Child, R.; Ramesh, A.; Ziegler, D. M.; Wu, J.; Winter, C.; Hesse, C.; Chen, M.; Sigler, E.; Litwin, M.; Gray, S.; Chess, B.; Clark, J.; Berner, C.; McCandlish, S.; Radford, A.; Sutskever, I.; and Amodei, D. 2020. Language models are few-shot learners. *Advances in Neural Information Processing Systems*, 2020-Decem.

Chen, X.; Men, K.; Li, Y.; Yi, J.; and Dai, J. 2019. A feasibility study on an automated method to generate patient-specific dose distributions for radiotherapy using deep learning. *Medical Physics*, 46(1): 56–64.

Cordonnier, J.-B.; Loukas, A.; and Jaggi, M. 2019. On the Relationship between Self-Attention and Convolutional Layers.

D'Ascoli, S.; Touvron, H.; Leavitt, M.; Morcos, A.; Biroli, G.; and Sagun, L. 2021. ConViT: Improving Vision Transformers with Soft Convolutional Inductive Biases.

Devlin, J.; Chang, M. W.; Lee, K.; and Toutanova, K. 2019. BERT: Pre-training of deep bidirectional transformers for language understanding. *NAACL HLT 2019 - 2019 Conference of the North American Chapter of the Association for Computational Linguistics: Human Language Technologies - Proceedings of the Conference*, 1(Mlm): 4171–4186.

Dong, P.; and Xing, L. 2020. Deep DoseNet: a deep neural network for accurate dosimetric transformation between different spatial resolutions and/or different dose calculation algorithms for precision radiation therapy. *Physics in Medicine & Biology*, 65(3): 035010.

Dosovitskiy, A.; Beyer, L.; Kolesnikov, A.; Weissenborn, D.; Zhai, X.; Unterthiner, T.; Dehghani, M.; Minderer, M.; Heigold, G.; Gelly, S.; Uszkoreit, J.; and Houlsby, N. 2020. An Image is Worth 16x16 Words: Transformers for Image Recognition at Scale.

Edmund, J. M.; and Nyholm, T. 2017. A review of substitute CT generation for MRI-only radiation therapy. *Radiation oncology (London, England)*, 12(1): 28.

Fan, J.; Wang, J.; Chen, Z.; Hu, C.; Zhang, Z.; and Hu, W. 2019. Automatic treatment planning based on three-dimensional dose distribution predicted from deep learning technique. *Medical Physics*, 46(1): 370–381.

Fan, J.; Xing, L.; Dong, P.; Wang, J.; Hu, W.; and Yang, Y. 2020. Data-driven dose calculation algorithm based on deep U-Net. *Physics in Medicine & Biology*, 65(24): 245035.

Ferlay, J.; Ervik, M.; Lam, F.; Colombet, M.; Mery, L.; Piñeros, M.; Znaor, A.; Soerjomataram, I.; and Bray, F. 2020. Global Cancer Observatory: Cancer Today.

Goodfellow, I.; Pouget-Abadie, J.; Mirza, M.; Xu, B.; Warde-Farley, D.; Ozair, S.; Courville, A.; and Bengio, Y. 2014. Generative Adversarial Nets. In Ghahramani, Z.; Welling, M.; Cortes, C.; Lawrence, N.; and Weinberger, K. Q., eds., *Advances in Neural Information Processing Systems*, volume 27. Curran Associates, Inc.

Harms, J.; Lei, Y.; Wang, T.; Mcdonald, M.; Ghavidel, B.; and Stokes, W. 2020. Cone-beam CT-derived relative stopping power map generation via deep learning for proton radiotherapy. 47(9): 4416–4427.

Hassani, A.; Walton, S.; Shah, N.; Abuduweili, A.; Li, J.; and Shi, H. 2021. Escaping the Big Data Paradigm with Compact Transformers.

Hendrycks, D.; and Gimpel, K. 2016. Gaussian Error Linear Units (GELUs). 1–9.

Hussein, M.; Heijmen, B. J. M.; Verellen, D.; and Nisbet, A. 2018. Automation in intensity modulated radiotherapy treatment planning—a review of recent innovations. *The British Journal of Radiology*, 91(1092): 20180270.

Javaid, U.; Souris, K.; Huang, S.; and Lee, J. A. 2021. Denoising proton therapy Monte Carlo dose distributions in multiple tumor sites: A comparative neural networks architecture study. *Physica Medica*, 89(August): 93–103.

Kajikawa, T.; Kadoya, N.; Ito, K.; Takayama, Y.; Chiba, T.; Tomori, S.; Nemoto, H.; Dobashi, S.; Takeda, K.; and Jingu, K. 2019. A convolutional neural network approach for IMRT dose distribution prediction in prostate cancer patients. *Journal of Radiation Research*, 60(5): 685–693.

Kearney, V.; Chan, J. W.; Haaf, S.; Descovich, M.; and Solberg, T. D. 2018. DoseNet: a volumetric dose prediction algorithm using 3D fully-convolutional neural networks. *Physics in Medicine & Biology*, 63(23): 235022.

Kontaxis, C.; Bol, G. H.; Lagendijk, J. J. W.; and Raaymakers, B. W. 2020. DeepDose: Towards a fast dose calculation engine for radiation therapy using deep learning. *Physics in Medicine & Biology*, 65(7): 075013.

Lalonde, A.; Winey, B.; Verburg, J.; Paganetti, H.; and Sharp, G. C. 2020. Evaluation of CBCT scatter correction using deep convolutional neural networks for head and neck adaptive proton therapy. *Physics in Medicine & Biology Biology*, 65(24): 245022.

Lee, H.; Kim, H.; Kwak, J.; Kim, Y. S.; Lee, S. W.; Cho, S.; and Cho, B. 2019. Fluence-map generation for prostate intensity-modulated radiotherapy planning using a deep-neural-network. *Scientific Reports*, 9(1): 15671.

Low, D. A.; Harms, W. B.; Mutic, S.; and Purdy, J. A. 1998. A technique for the quantitative evaluation of dose distributions. *Medical Physics*, 25(5): 656–661.

Lundkvist, J.; Ekman, M.; Ericsson, S. R.; Jönsson, B.; and Glimelius, B. 2005. Proton therapy of cancer: Potential clinical advantages and cost-effectiveness. *Acta Oncologica*, 44(8): 850–861.

Meyer, P.; Noblet, V.; Mazzara, C.; and Lallement, A. 2018. Survey on deep learning for radiotherapy. *Computers in Biology and Medicine*, 98(May): 126–146.

Neishabouri, A.; Wahl, N.; Mairani, A.; Köthe, U.; and Bangert, M. 2021. Long short-term memory networks for proton dose calculation in highly heterogeneous tissues. *Medical Physics*, 48(4): 1893–1908.

Neph, R.; Lyu, Q.; Huang, Y.; Yang, Y. M.; and Sheng, K. 2021. DeepMC: a deep learning method for efficient Monte Carlo beamlet dose calculation by predictive denoising in magnetic resonance-guided radiotherapy. *Physics in Medicine & Biology*, 66(3): 035022.

Nguyen, D.; Jia, X.; Sher, D.; Lin, M.-H.; Iqbal, Z.; Liu, H.; and Jiang, S. 2019a. 3D radiotherapy dose prediction on head and neck cancer patients with a hierarchically densely connected U-net deep learning architecture. *Physics in Medicine & Biology*, 64(6): 065020.

Nguyen, D.; Long, T.; Jia, X.; Lu, W.; Gu, X.; Iqbal, Z.; and Jiang, S. 2019b. A feasibility study for predicting optimal radiation therapy dose distributions of prostate cancer patients from patient anatomy using deep learning. *Scientific Reports*, 9(1): 1076.

Peng, Z.; Shan, H.; Liu, T.; Pei, X.; Wang, G.; and Xu, X. G. 2019a. MCDNet – A Denoising Convolutional Neural Network to Accelerate Monte Carlo Radiation Transport Simulations: A Proof of Principle With Patient Dose From X-Ray CT Imaging. *IEEE Access*, 7: 76680–76689.

Peng, Z.; Shan, H.; Liu, T.; Pei, X.; Zhou, J.; Wang, G.; and Xu, X. G. 2019b. Deep learning for accelerating Monte Carlo radiation transport simulation in intensity-modulated radiation therapy. 1–8.

Pereira, G. C.; Traughber, M.; and Muzic, R. F. 2014. The Role of Imaging in Radiation Therapy Planning: Past, Present, and Future. *BioMed Research International*, 2014(2): 1–9.

Ramachandran, P.; Bello, I.; Parmar, N.; Levskaya, A.; Vaswani, A.; and Shlens, J. 2019. Stand-alone self-attention in vision models. *Advances in Neural Information Processing Systems*, 32.

Ronneberger, O.; Fischer, P.; and Brox, T. 2015. U-Net: Convolutional Networks for Biomedical Image Segmentation. In Navab, N.; Hornegger, J.; Wells, W. M.; and Frangi, A. F., eds., *Medical Image Computing and Computer-Assisted Intervention – MICCAI 2015*, 234–241. Cham: Springer International Publishing. ISBN 978-3-319-24574-4.

Souris, K.; Lee, J. A.; and Sterpin, E. 2016. Fast multipurpose Monte Carlo simulation for proton therapy using multi- and many-core CPU architectures. *Medical Physics*, 43(4): 1700–1712.

Srivastava, N.; Hinton, G.; Krizhevsky, A.; and Salakhutdinov, R. 2014. Dropout: A Simple Way to Prevent Neural Networks from Overfitting. *Journal of Machine Learning Research*, 15: 1929–1958.

Sung, H.; Ferlay, J.; Siegel, R. L.; Laversanne, M.; Soerjomataram, I.; Jemal, A.; and Bray, F. 2021. Global Cancer Statistics 2020: GLOBOCAN Estimates of Incidence and Mortality Worldwide for 36 Cancers in 185 Countries. *CA: A Cancer Journal for Clinicians*, 71(3): 209–249.

Touvron, H.; Cord, M.; Douze, M.; Massa, F.; Sablayrolles, A.; and Jégou, H. 2020. Training data-efficient image transformers & distillation through attention. 1–22.

Tsekas, G.; Bol, G. H.; Raaymakers, B. W.; and Kontaxis, C. 2021. DeepDose: a robust deep learning-based dose engine for abdominal tumours in a 1.5 T MRI radiotherapy system. *Physics in Medicine & Biology*, 66(6): 065017.

Vaswani, A.; Shazeer, N.; Parmar, N.; Uszkoreit, J.; Jones, L.; Gomez, A. N.; Kaiser, Ł.; and Polosukhin, I. 2017. Attention is all you need. In *Advances in Neural Information Processing Systems*, volume 2017-Decem, 5999–6009.

Wang, W.; Sheng, Y.; Wang, C.; Zhang, J.; Li, X.; Palta, M.; Czito, B.; Willett, C. G.; Wu, Q.; Ge, Y.; Yin, F.-F.; and Wu, Q. J. 2020. Fluence Map Prediction Using Deep Learning Models – Direct Plan Generation for Pancreas Stereotactic Body Radiation Therapy. *Frontiers in Artificial Intelligence*, 3(September): 1–10.

Wieser, H. P.; Cisternas, E.; Wahl, N.; Ulrich, S.; Stadler, A.; Mescher, H.; Muller, L. R.; Klinge, T.; Gabrys, H.; Burigo, L.; Mairani, A.; Ecker, S.; Ackermann, B.; Ellerbrock, M.; Parodi, K.; Jakel, O.; and Bangert, M. 2017. Development of the open-source dose calculation and optimization toolkit matRad. *Medical Physics*, 44(6): 2556–2568.

Wu, C.; Nguyen, D.; Xing, Y.; Montero, A. B.; Schuemann, J.; Shang, H.; Pu, Y.; and Jiang, S. 2021. Improving proton dose calculation accuracy by using deep learning. *Machine Learning: Science and Technology*, 2(1): 015017.

Wu, Y.; and He, K. 2020. Group Normalization. *International Journal of Computer Vision*, 128(3): 742–755.

Xing, Y.; Nguyen, D.; Lu, W.; Yang, M.; and Jiang, S. 2020a. Technical Note: A feasibility study on deep learning-based radiotherapy dose calculation. *Medical Physics*, 47(2): 753–758.

Xing, Y.; Zhang, Y.; Nguyen, D.; Lin, M.; Lu, W.; and Jiang, S. 2020b. Boosting radiotherapy dose calculation accuracy with deep learning. *Journal of Applied Clinical Medical Physics*, 21(8): 149–159.

You, Y.; Li, J.; Reddi, S.; Hseu, J.; Kumar, S.; Bhojanapalli, S.; Song, X.; Demmel, J.; Keutzer, K.; and Hsieh, C.-J. 2019. Large Batch Optimization for Deep Learning: Training BERT in 76 minutes.

Zhang, Y.; Yue, N.; Su, M.-y.; Liu, B.; Ding, Y.; Zhou, Y.; Wang, H.; Kuang, Y.; and Nie, K. 2021. Improving CBCT quality to CT level using deep learning with generative adversarial network. *Medical Physics*, 48(June): 2816–2826.

Zhu, J.; Liu, X.; and Chen, L. 2020. A preliminary study of a photon dose calculation algorithm using a convolutional neural network. *Physics in Medicine & Biology*, 65(20): 20NT02.